Research Article

AgNPs@ZnO hybride nanoparticles infused thermoplastic polyester elastomer and their biocide effect

Duclerc Fernandes Parra[1] · Leonardo Guedes Marchini[1] · Luiz Gustavo Hiroki Komatsu[1] · Camila Bassetti de Oliveira[1] · Washington Luiz Oliani[1] · Vijaya Kumar Rangari[2]

Received: 14 December 2020 / Accepted: 10 February 2021 / Published online: 1 March 2021

Abstract
This paper presents research results of biocidal effect of thermoplastic- polyester-elastomer (TPE-E) with incorporation of hybrid Ag/ZnO/SiO_2 NPs (silver/Zinc oxide/SiO_2 nanoparticles). These results were compared with various gamma-irradiated doses and processing techniques including extrusion, injection molding and compression molding. In all these processing techniques the TPE-E was mixed with mineral oil and Ag/ZnO/SiO_2 nanoparticles. The TPE-E nanocomposites were characterized by differential scanning calorimetry (DSC), thermogravimetry analysis (TGA), Infrared FT spectroscopy (FTIR), surface enhanced Raman technique **(**SERS), FESEM (Field emission scanning electron microscopy), Energy-dispersive X-ray spectroscopy (EDS), X-ray diffraction (XRD), TEM (transmission electronic microscopy) and antimicrobial test. Antibacterial activity against *E. coli* and *S. aureus*, are reported and these results showed potential application in health care products.

Keywords TPE · Silver nanoparticles · Processing · Antibacterial · Gamma-irradiation

1 Introduction

Polyolefin TPEs are distinguished from other polyolefins by a lower overall crystallinity and a higher amount of extensible amorphous regions [1].

The TPE-Es are slightly hygroscopic due to their polar character, besides being resistant to hydrolysis [3].

While usually rubbers are "vulcanized" or crosslinked through covalent bonds, TPEs are interesting materials because they have rubber properties without crosslinking [1, 2]. Since their inception in the 1960s, thermoplastic elastomers (TPEs) are being increasingly considered for a range of applications including automotive, medical equipment, and aeronautics [4–6].The main advantages of TPE-E are that they can be processed as thermoplastics using traditional techniques such as injection molding, compression molding, and extrusion. TPE-E properties, mainly their mechanical and thermal properties, are not as good as those of elastomers. For improvement of properties, TPE-E specimens with and without a crosslinking agent at high irradiation doses were studied [7]. The TPE-E polymer is used in several medical devices owing to the compatibility with human blood and tissue, for example, catheter, valves, syringe, surgical instruments, wound dressing, etc. It has inherent stability under radiation used for sterilization [3]. Nowadays, infection with pathogenic microorganisms contamination is a major concern in hospitals, from textiles to surgical pieces of equipment, from masks to catheters [8]. Infections are combated with antimicrobial agents but a rapid mutation in their genes creates resistance in operating antibiotic treatments [9]. It was estimated that 10% (2018) of hospitalized patients

✉ Duclerc Fernandes Parra, parduclerc@yahoo.com.br | [1]Nuclear and Energy Research Institute, IPEN, CNEN/SP, Av. Prof. Lineu Prestes, 2242 –Cidade Universitária CEP, São Paulo 05508-000, Brazil. [2]Department of Materials Science and Engineering, Tuskegee University, Tuskegee, AL, USA.

were diagnosed with some type of infection during the period of hospitalization, under the large types of infections in the hospital environment. WHO (World-Health-Organization) reports registered that usually public attention on health-care-associated- infections (HCAIs) are only attempted in epidemic periods when HCAIs impacted at around 0.5 million cases of "critically ill patients with of HCAIs being diagnosed every year in intensive-care-units (ICUs)" [10]. The most frequent infections are respiratory infections (19% of cases) by catheter (13% of cases), urinary infection (34% of cases), and suture infection (17% of cases) [11].

Antimicrobial polymer composites are expected to participate more and more in human life in projecting materials against the microorganisms (bacteria, viruses, and fungi). Technology has been developed for direct deposition of an antimicrobial agent or for coating the surface of the polymer, or as for surface modification by ionizing radiation [12].

The nanotechnology of polymers and antimicrobials is an important strategy to be applied for different polymer processing techniques by several methods as compression, extrusion, injection, or blow extrusion. The advantage of this embodiment is that owing to the low concentrations of the agent, process parameters do not require significant modifications in the maintenance of the mechanical properties of the final compound [13, 14]. Results of the concept can be cited as for example: AgNPs with polyamide (PA) [15], polypropylene (PP) AgNPs nanocomposites [16], and AgNPs nanocomposites with polyethylene (PE) [17]. Gamma irradiation is also applied in the production of polymers-AgNPs [18]. High-melting-strength-polypropylene (HMSPP), an irradiation modified polypropylene improved by long-chain-branched (LCB) favors processing via extrusion, and with added of AgNPs produce films with biocidal properties[16].

Silver nanoparticles infused in thermoplastic-elastomer (TPE), such as thermoplastic-polyurethane (TPU) [19] and TPE based on (SEBS) were reported in the literature [20].

Tomacheski and et al. studied the antibacterial action of the SEBS thermoplastic elastomers loaded with silver nanoparticle on silica pyrogenic additives, silver phosphate glass, and silver bentonite differently mixed. The compounds showed antimicrobial activity against *E. coli* and *S. aureus*. All of the additives eliminated more than 90% of *E.coli*, but only AgNPs silica killed more than 80% of the *S. aureus* population. The authors concluded that the best effect of AgNP@silice was attributed to the high specific surface area of the additive, which promoted greater contact with bacteria cells [21].In other work, Pittol reports the evaluation of the antimicrobial activity of TPE compounds against *S. aureus*, *E.coli* and the antifungal action against *Aspergillus niger*, *Candida albicans* and *Cladosporium cladosporioides*. Specimes prepared with zinc pyrithionate eliminated almost 100% of *E. coli* and *S. aureus* population and showed a zone of inhibition in the fungal assay [22].Concerning the processability of nanosilver in polymers, processes of melt dispersion and extrusion produced masterbatches of nanocomposites of LDPE and PP containing silver nanoparticles. Both nanocomposites in films were active against *E. coli* and *S. aureus* at concentrations of 36–30 mg kg^{-1} of silver nanoparticles for AgNPs/LDPE and AgNPs/PP films, resulting in a total decrease in the bacteria viability [17]. AgNPs in ZnO nanoparticles is an important antibacterial agent with varied morphology, large surface area to volume ratio, potent antibacterial activity, and biocompatibility.

In recent work, the antibacterial potential of silver nanoparticles using ampicillin was investigated against sensitive and drug-resistant bacteria [23]. The results indicated that bacterial strains do not show any resistance to Ampicillin@AgNPs even after exposure up to 15 successive cycles [24], corroborating our interest in developing AgNPs based on antimicrobials.

The present work reports the microbiological effects of AgNPs@ZnO/SiO_2, nanoparticles in thermoplastic elastomeric composite obtained from different processing techniques: extrusion, compression and injection and radiation. To our knowledge, there are no study reported in the literature, on the bactericidal activity of AgNPs in thermoplastic-polyester-elastomer (TPE-E) compounds, using gamma-radiation. In the present study, we reported the antimicrobial activity and efficacy with strains of *Staphylococcus aureus* and *Escherichia coli*. For both strains the higher activity showed for the TPE-E nanocomposites resulted from gamma-radiation processed composites.

2 Materials and methods

2.1 Materials

The materials used were: The TPE-E, melt flow index (MFI) is 10 g/10 min (230 °C, 2.16 kg), density: 1.20 g cm^{-3}, Mn = 57,500 g mol^{-1} and Mw = 115,000 g mol^{-1}supplied by Celanese, Fig. 1; Antioxidant Irganox®B215 ED, 67% tris(2,4- ditert-butylphenyl)phosphate, 33%

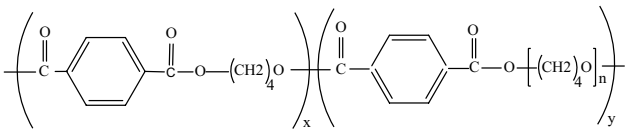

Fig. 1 Chemical structure of TPE-E [25–27] *x* = PBT—poly(butylene terephthalate) *y* = PTMO – poly(tetramethylene oxide)

pentaerythritoltetrakis[3-[3,5-di-tert-butyl-4- hydroxyphenyl]propionate] from BASF; mineral oil Alkest TW80 from Oxiteno, Fig. 2, composed synthetized by ethoxylated-sorbitan-esters. The nanoparticles were composed by zinc oxide added of colloidal dispersion of metallic silver adsorbed on silica pyrogen, from TNS Ltda. Before the processing, the TPE-E, pellets were dried at 100 °C for 24 h.

The TPE-E, aromatic semicrystalline polycondensation polymer, is composed by crystalline rigid part of poly(butylene terephthalate) (PBT) and combination with amorphous and elastic part composed of poly(tetramethylene oxide) (PTMO).

TPE-E is a partially crystalline polymer because the rigid part composed of poly(butylene-terephthalate) (PBT), and the flexible part, amorphous phase, of poly(tetramethylene oxide)(PTMO). The degree of crystallinity (Xc) of the compound was determined using the experimental heat of fusion (ΔHm) taking into account the fraction of PBT in the copolymer (ΔHPBT). The degree of crystallinity of pristine TPE-E was 11.1% and melting temperature of 199.8 °C of the PBT crystals. The TPE-E used in the study has percentage of PBT of 58%, according to the supplier [28].

Where: R = alkyl group.

w + x + y + z = average moles of ethoxylation.

Eight different formulations containing the TPE-E were prepared and are represented in Table 1.

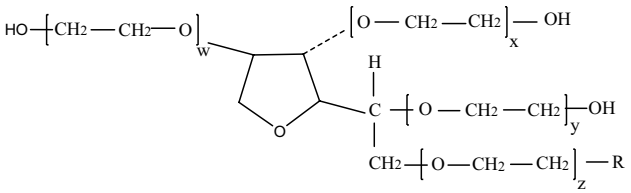

Fig. 2 Chemical structure of mineral oil Alkest TW80 [32]

2.2 Process conditions

2.2.1 Extrusion

2.2.1.1 Processing conditions The TPE-E in pellet was mixed with mineral oil and Irganox B 215 ED in a rotary mixer at room temperature of (25 ± 2)°C and maintained under this condition for 12 h. Then the mixture was processed in a twin-screw-extruder Thermo Haake, model Rheomex OS PTW 16/25, with the following processing conditions: the temperature profile for the six sections of the twin barrel was set to 185, 190, 195, 200, 205 °C and 210 °C with screw rotating speed of 100 rpm. The samples were cut in pellet and the material was placed directly into the hopper of the extruder with a temperature profile (feed to die) of 185–210 °C, screw speed of 20 rpm and torque of 40–53 Nm. Planar-sheet-extruder transformed the material to TPE-E films with a thickness of 0.08 mm approximately.

2.2.2 Compression molding

The specimen of TPE-ENC obtained by extrusion were molded and hot pressed under the following conditions: temperature 210 °C and 60 bar pressure for 10 min, followed by 210 °C and 80 bar pressure for a further 5 min. The obtained films thermo-pressed were cooled at (25 ± 2)°C. The blends were subjected to gamma radiation at ambient conditions. The irradiation of films was carried out by using a ^{60}Co gamma rays unit installed at the IPEN-CTR, Brazil. The as prepared samples were irradiated at 20 and 50 kGy at a dose rate of 5 kGy h^{-1}.

2.2.3 Injection molding compounder

The masterbatch TPE-ENC followed for molding in a 5ton injection-molding- machine (Arburg Golden). Molding

Table 1 Composition of TPE-ENC nanocomposite formulations (wt%)

Sample	Matrix	Irganox(%)	Dose(kGy)	AgNP@ZnO/SiO_2(%)	Processing Techniques
TPE-E Pristine	TPE-E	1	–	–	EXT/CM/INJ
TPE-ENC1	TPE-E	1	–	0.05	EXT
TPE-ENC2	TPE-E	1	–	0.5	EXT
TPE-ENC3	TPE-E	1	–	0.5	CM
TPE-ENC4	TPE-E	1	20	0.5	CM
TPE-ENC5	TPE-E	1	50	0.5	CM
TPE-ENC6	TPE-E	1	–	0.05	INJ
TPE-ENC7	TPE-E	1	–	0.5	INJ

1:0.05/EXT; 2:0.5/EXT; 3:0.5/CM; 4:0.5/CM20; 5:0.5/CM50; 6:0.05/INJ; 7:0.5/INJ

EXT Extrusion; *CM* Compression molding; *INJ* Injection molding; *TPE-ENC* Thermoplastic-Polyester-Elastomer-Nanocomposite

conditions were set to injection conditions assuming, injection speed of 100 mm s^{-1}, holding pressure of 480 MPa, resin temperature of 200–210 °C, and mold temperature of 50 °C. The injection molded specimens were prepared according to ISO 527–1: 2019 [29].

2.3 Characterization methods

2.3.1 Differential scanning calorimetry

Heat of enthalpy of specimens was characterized using a Mettler Toledo DSC 822^e differential scanning calorimeter. The thermal program used for polymer nanocomposite films was: step heating from − 50 to 280 °C at a heating rate of 10 °C min^{-1} under nitrogen atmosphere; step holding for 5 min at 280 °C, step cooling to − 50 °C and step reheating to 280 °C at 10 °C min^{-1}.The degree of crystallinity of TPE-E was assessed using given Eq. (1):

$$X_c = \frac{\Delta Hm}{W_h} \times \left(\Delta H_{PBT}\right)^{-1} \times 100\%$$

$$x(\Delta H_{PBT})^{-1} \times 100\% \quad (1)$$

Degree of crystallinity *Xc* considers the melting enthalpy (ΔHm) of the PBT, 100% of crystal phase, as 145 Jg^{-1} [30, 31], and Wh the fraction of PBT used in the reaction of the mixture.

2.3.2 Thermogravimetry analysis

Thermogravimetry analysis were carrid out using TGA/SDTA 851 thermobalance (Mettler-Toledo), using 10 mg of samples in appropriated pans, in the range from 25 up to 600 °C, at heating rate of 10 °C min^{-1}. The atmosphere used was N_2, at 50 mL min^{-1}.

2.3.3 Infrared spectroscopy—FTIR

The spectroscopic analysis of all the samples were recorded using on the Perkin Elmer Frontier™ spectrometer in the wavelength range 4000 cm^{-1}–600 cm^{-1}, single reflection of total reflectance (ATR) accessory.

2.3.4 Raman spectroscopy—SERS

Raman spectroscopic characterizations were performed using the Raman laser 785 nm, InPhotonics.

2.3.5 Field emission scanning electron microscopy and energy-dispersive spectroscopy – FESEM/EDS

The samples TPE-E were fixed in appropriate holder and coated with a gold layer. The samples were analyzed by *FESEM/EDS* microscopy with field emission, from JEOL FESEM, JSM-6701F, Japan, using the accelerating voltage of 6.0kVA.

2.3.6 X-ray diffraction—XRD

X-ray diffraction (XRD) measurements were carried out on a Rigaku diffractometer Mini Flex II (Tokyo, Japan) operated at 30 kV voltage. The specimens were prepared with dimensions of $(2.5 \times 2.5)cm^2$ and fixed on glass slides and recorded in the reflection mode under CuKα radiation (λ = 1.541,841 Å).

2.3.7 Transmission electron microscopy—TEM

The morphology of the samples was examined in transmission electron microscopy operating at voltage of 80 kV. Ultrathin Sects. (80 nm) were prepared with a Leica EM FC6 ultramicrotome with a diamond knife. The TEM equipment JEOL JEM-2100 was used for the images.

2.3.8 Antimicrobial activity

The antimicrobial activity and efficacy were evaluated according to adaptation of the standard JIS Z 2801:2010 [32]. Each of the microorganisms used was activated to the respective stock cultures in appropriate culture medium to obtain inoculate. The strains tested were: *Staphylococcus aureus* (ATCC 6538) and *Escherichia coli* (ATCC 3789). The cell suspension obtained for each step tested was standardized to obtain a final inoculum concentration of 10^5 CFU mL^{-1}.

A short description of the procedure was performed separately for the culture/sample to be tested: 0.4 mL of inoculums suspension was inserted over the specimen, previously sterilized with 70% alcohol, spread over an area corresponding to $(40 \times 40)mm^2$. It was then covered by a sterile coverslip and incubated in a sterile Petri dish for approximately 4 h at 37 °C. After the incubation time, 5 dilutions were made to allow colony counting. For each dilution, plating was performed using a Petri dish containing agar PCA and incubated at 37 °C for 24 h. The percentage of bacterial growth reduction was calculated from the amount of surviving bacteria found in the Petri dish.

3 Results and discussion

3.1 Thermal analysis characterization of composite polymers (DSC, TGA)

3.1.1 Differential scanning calorimetry

The Table 2 presents enthalpy results of melting temperature, Tm, melting enthalpy and crystallinity of TPE-E composites from different processes, after the second heating cycle.

Comparing all the samples in terms of crystallinity, it was observed one slightly decrease in the samples crystallinity between different processes. The specimens of the TPE-ENC5 are the unique with increased percentage crystallinity value probable by the radiation effect. Comparing with the lower dose irradiated sample and the other differently processed, the increase in the integral dose in all the materials resulted in higher enthalpic energy and the higher crystallinity (11.27%). The crystallinity degree increased with the higher dose of 50 kGy. This was attributed to polymer chain scissions produced by radiation, in which decreasing its molecular weight and generate defects, increases the crystallinity.

3.1.2 Thermogravimetry analysis

The TG results indicated the thermal decomposition of the samples, Table 3. The table reports decrease of stability for the samples containing nanosilver, in comparison to the TPE-E pristine.

The calculated T_{onset} reported changes in the degradation temperature of the samples containing nanosilver compared to pristine TPE-E. The lowest initial decomposition temperature (T_{onset}) was observed for TPE-ENC2 with 329.5 °C and TPE-ENC4 with 335.9 °C. The AgNPs@ZnO/SiO_2 when added in the polymer matrix both via single-screw-extruder, injection and compression molding brought thermal instability when compared to pristine TPE-E material but depends also, and more intensely of the nanosilver concentration. The irradiation process modified the stability at 20 kGy but is not intensified at 50 kGy and the silver concentration showed evidently more influence in the thermal stability of the films.

Table 2 DSC data of TPE-E samples during the second run of heating

Sample	T_m(°C)	$2^{nd}\Delta H_m$(J/g)	$2^{nd}X_c$(%)
TPE-E Pristine	199.8	25.89	10.40
TPE-ENC1	199.4	23.67	9.50
TPE-ENC2	200.2	25.26	10.10
TPE-ENC3	199.2	24.22	9.71
TPE-ENC4	198.9	24.04	9.65
TPE-ENC5	198.8	28.13	11.27
TPE-ENC6	198.4	24.53	9.80
TPE-ENC7	198.7	26.22	10.50

1:0.05/EXT; 2:0.5/EXT; 3:0.5/CM; 4:0.5/CM20; 5:0.5/CM50; 6:0.05/INJ; 7:0.5/INJ

TPE-ENC Thermoplastic-Polyester-Elastomer-Nanocomposite

Table 3 Initial decomposition temperature, T_{onset}, calculated from TG curves obtained under N_2 atmosphere, for TPE-E composites after processing

Sample	T_{onset} (°C)
TPE-E Pristine	362.4
TPE-ENC1	362.6
TPE-ENC2	329.5
TPE-ENC3	343.1
TPE-ENC4	335.9
TPE-ENC5	345.5
TPE-ENC6	359.3
TPE-ENC7	342.8

1:0.05/EXT; 2:0.5/EXT; 3:0.5/CM; 4:0.5/CM20; 5:0.5/CM50; 6:0.05/INJ; 7:0.5/INJ

3.2 Structure of composite polymers and films (FTIR, Raman, XRD)

3.2.1 Infrared Spectroscopy—FTIR

The spectrum interpretation of the infrared FTIR-ATR of the pristine TPE-E corresponds to the typical spectrum of a thermoplastic composed by PBT, Fig. 3.

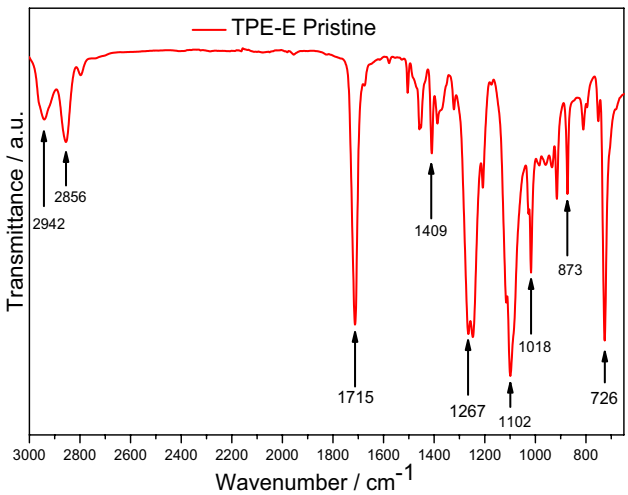

Fig. 3 FTIR-ATR spectra of pristine TPE-E

The Fig. 3 reports characteristics peaks attributed to chemical groups of TPE- E: anti-symmetric-stretching of (–CH2-) at 2942 cm^{-1}, symmetric stretching of (–CH2-) at 2856 cm^{-1}, carbonyl absorption band (C = O) at 1715 cm^{-1}, aromatic ring stretching absorption of (C = C–C) at 1409 cm^{-1}, band at 1267 cm^{-1} attributed to (C–C–O), absorption stretching of (O–C–C) at 1102 cm^{-1}, aromatic plane folding absorption (C–H) at 1018 and 873 cm^{-1}, rotation of (–CH2-) > 3 at 726 cm^{-1} according to the literature [33].

3.2.2 Raman spectroscopy—SERS

The Fig. 4 shows the Raman spectrum of the samples TPE-E.

The formation of pure Wurtzite hexagonal phase of ZnO was confirmed by Raman characterization. As show in Fig. 4a, it was reported two obvious peaks at 382 and 440 cm^{-1}, results that corroborated with the literature [34, 35]. The peaks at 1358 cm^{-1} and 1589 cm^{-1} were attributed to the enhancement of Raman lines by carbon polymeric segments [36, 37].

3.2.3 Field emission scanning electron microscopy and energy-dispersive spectroscopy—FESEM/EDS

The Fig. 5 shows the SEM images and EDS for TPE-ENC (Fig. 6).

3.2.4 X-ray diffraction—XRD

XRD patterns of the TPE-E sample showed peaks in the interval of 2θ = 5–35° characteristic of the polymer structure, are given in Fig. 7.

The pristine TPE-E shows intense peaks at 2θ = 16.4, 17.7, 21.1, 23.8 and 25.4° which are from PBT. These peaks represent the diffraction planes of [011], [010], [111], [100] and [111], respectively. The PBT presents two α and β crystalline phases, the β phase being formed due to mechanical deformation recorded at 2θ = 29 and 31 degrees [30].

XRD patterns of the TPE-ENC specimens were identified by diffraction angles which characteristic for the structure of polymer are given in Figs. 8, 9 and 10.

The insets show XRD pattern for the prepared Ag@ZnO/SiO_2 nanoparticles and Ag@ZnO, for identification of the nanoparticles.

The insets showed in XRD pattern for the prepared Ag@ZnO nanoparticles corroborated to the identification of the nanoparticles of Ag and Zn, in the films.

It is observed in the Fig. 9, the presence of nanoparticles of ZnO in both irradiated and not irradiated films obtained by molding.

Diffraction peak corresponding to the ZnO hexagonal phase, the relative intensity of the diffraction peaks corresponds to the reference diffractogram, presenting a preferential orientation according to the diffraction plane (002) in 2θ = 34.4°, [38].

The crystallite size and lattice strain were reduced and modified by gamma radiation affecting the Bragg peak [39]. Both these effects extend the peak width and

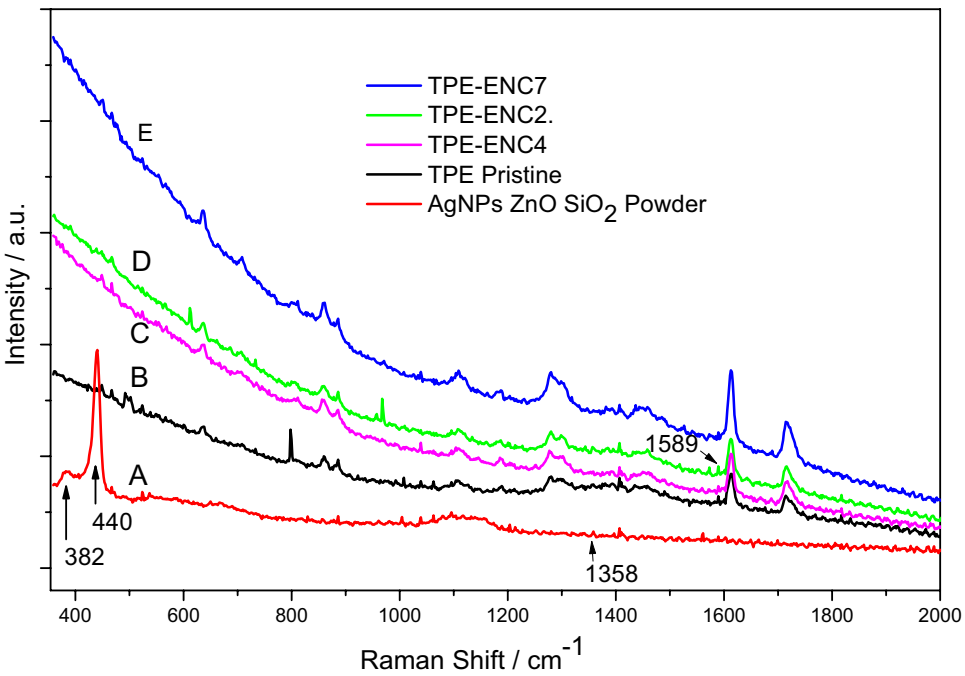

Fig. 4 Raman spectrum of TPE-E samples: (**a**) AgNPs@ZnO/SiO_2 Powder; (**b**) TPE-E Pristine; (**c**) TPE-ENC4; (**d**) TPE-ENC2 and (**e**) TPE-ENC7

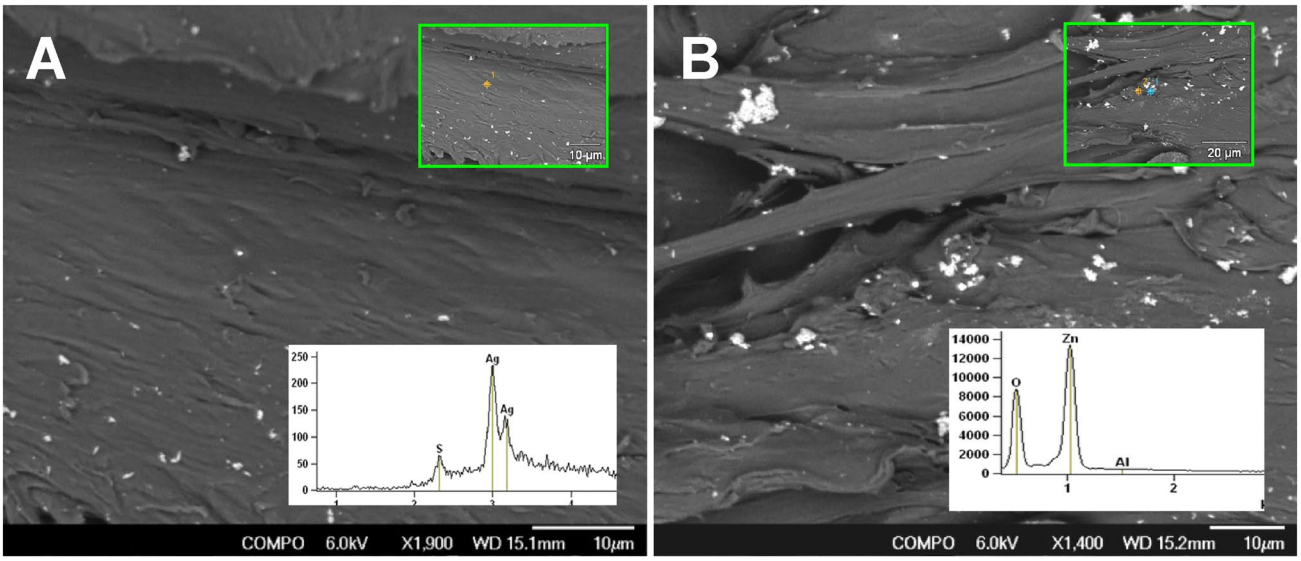

Fig. 5 FESEM image of the obtained film by extrusion on fracture TPE-ENC2 (**a**) and FESEM image of the obtained film by extrusion on surface TPE-ENC2 (**b**).The images in the inset show EDS of Ag and Zn elements

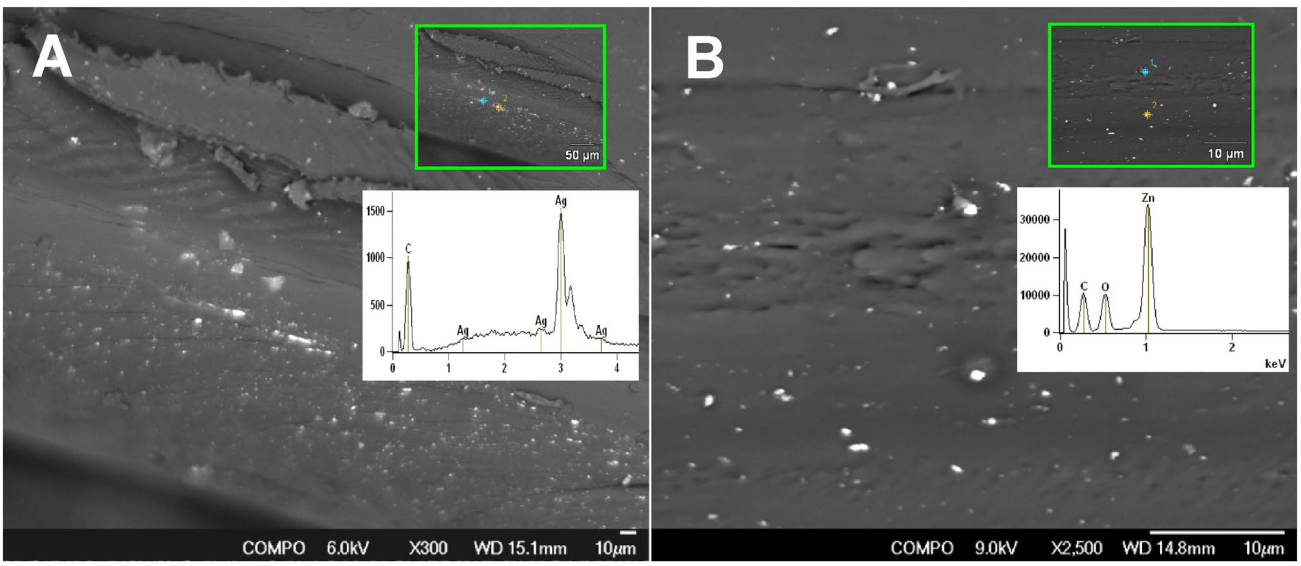

Fig. 6 FESEM image of the obtained film by compression molding on fracture TPE-ENC3 (**a**) and FESEM image of the sample fracture obtained by injection, TPE-ENC7 (**b**).The images in the inset show EDS with identification Ag and Zn elements. Figure 5a shows the micrograph of the film obtained by extrusion and fractured in nitrogen. Ag° clusters are observed and identified by EDS. Figure 5b shows the micrograph of the surface obtained by extrusion in which EDS identified Zn in white clusters. Figure 6a shows the micrograph of fractured surface of the film obtained by compression molding, EDS identified Ag° agglomerates. Figure 6b shows the micrograph of fracture surface of sample obtained identifying Zn agglomerates

intensity and shift the peak position, as observed in sample TPE-ENC4, Fig. 9. The crystallite size tends to be reduced by gamma radiation dose from 20 to 50 kGy. The irradiation of the samples showed a tendency to chain scission in the amorphous part and in consequence promoted slightly increase in the cristallinite (%) [40], as observed after irradiation at 50 kGy.

Figure 10 shows the XRD patterns of the nanocomposite films TPE-E6 and TPE-E7 (AgNPs@ZnO) by injection molding process. The inset on Fig. 10 compares the AgNPs@ZnO powder diffractogram for attribution of the metal peaks at films of TPE-E6 and TPE-E7 (AgNPs@ZnO).

The samples of the compounds TPEE-ENC1 and TPE-ENC2 obtained by extrusion, by injection the TPE-ENC7

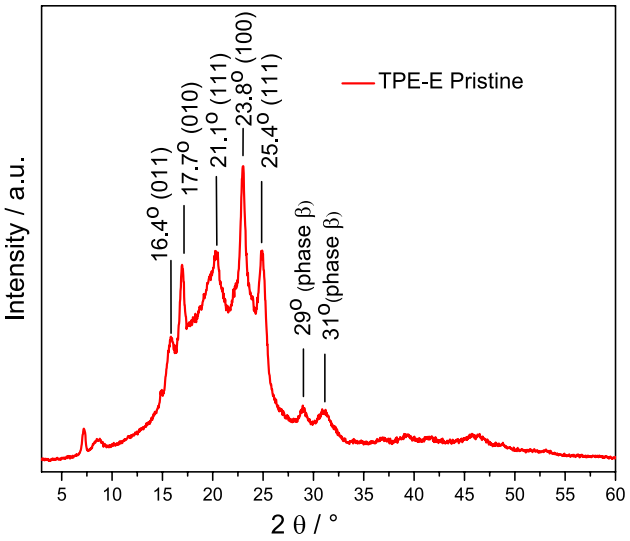

Fig. 7 X-ray diffraction patterns of TPE-E pristine film

and sample obtained by thermopressed molding TPE-ENC4 showed, in the surface, presence of the ZnO by peaks around 31.8, 34.4°, 36.3 and 56.5° assigned to their respective crystalline planes [100], [002], [101], [110], as described by [39–42]. These results match very well with the Joint Committee on Powder Diffraction Standards (JCPDS) of ZnO (JCPDS#36-1451). Peak displacement occurred at around 25.5° with respect with the pristine TPE-E sample.

Double peaks at around 29 and 31° are related to the β phase, become absent as does the peak at 7 and 24.5°. The SiO_2 related peak present in the compound containing AgNPs@ ZnO/SiO_2 is found at 21° where the intensity increases with the concentration, as can be seen at insert in the Fig. 8. It was also found at 38.5 and 44.5° peaks corresponding to the crystalline planes of silver [111] and [200], respectively, according research. The wide peak at 22.5° represents the amorphous phase of SiO_2 [44].

3.3 Morphology: composition of composite polymers and films (TEM, FESEM/EDS)

3.3.1 Transmission electron microscopy – TEM

TEM micrographs of the Ag@ZnO-NPs was presented in Fig. 11.

The morphology was found to be irregular as confirmed in the images. Rectangular and rod morphologies are represented by ZnO, similar morphology found by Bakhori et al. [45] and spherical by Si and Ag as shown in the Fig. 12a and b. The format of the most efficient Ag for bactericidal activity is the spherical form [46, 47]. The geometric particles size based on TEM micrographs reveals the

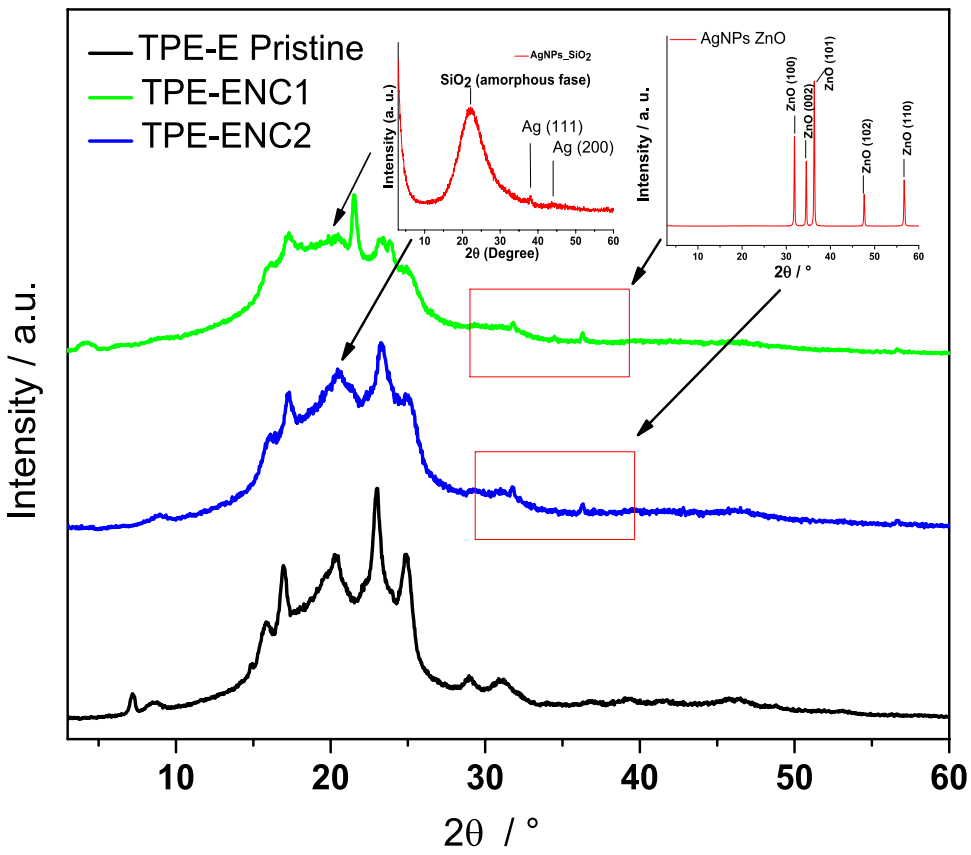

Fig. 8 XRD Diffractograms of films from extrusion of: Pristine TPE-E; TPE- ENC1 and TPE-ENC2 with AgNPs@ZnO/SiO_2

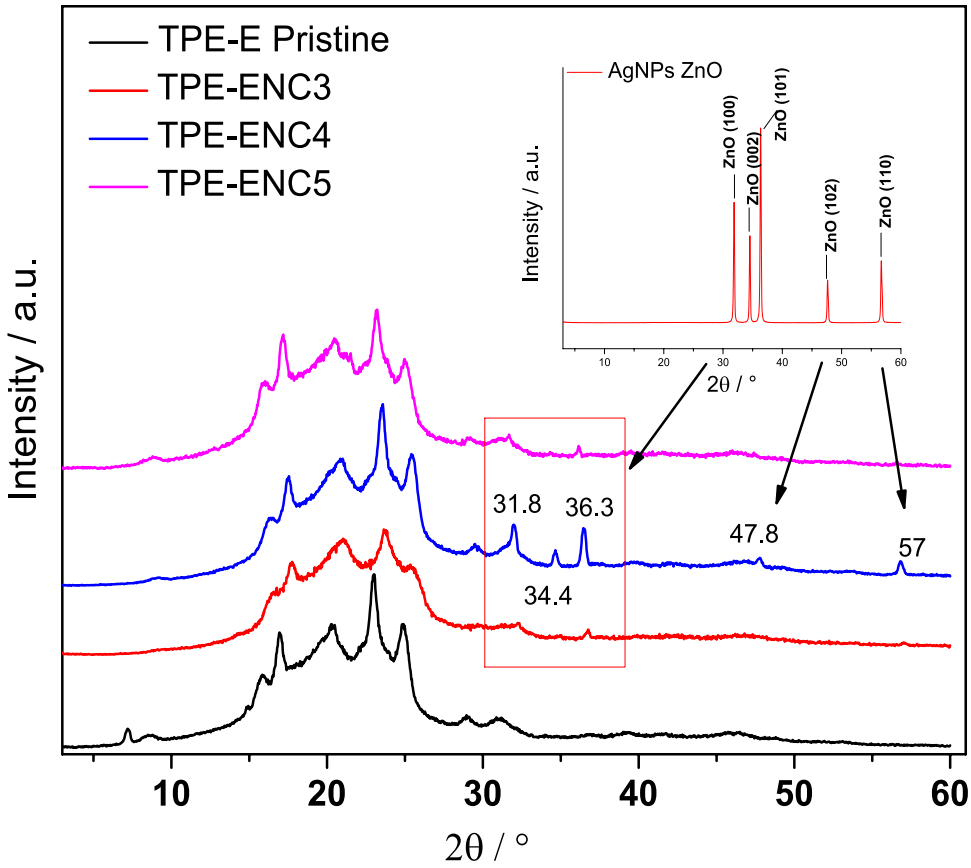

Fig. 9 XRD Diffractograms of films from compression molding of: Pristine TPE- E, TPE-NC3 and the films irradiated at 20 kGy, TPE-ENC4 and 50 kGy, TPE- ENC5

smallest rectangular particle side of (ZnO) size measuring approximately 100 nm. The structure of ZnO is predominant in Fig. 11, but smallest spheres refer to Ag that has been introduced in the agglomerate.

TEM image of sample Ag nanoparticles produced in composite characterized a predominant spherical morphology and anchored in substract of SiO_2. Figure 12a shows the spherical shape of the AgNPs and the formation of agglomerates in the TPE-E film. The size of the AgNPs ranged from 45 to 50 nm in diameter with anchoring on SiO_2, and Fig. 12b the nanosilver showed a size of 15 nm.

3.4 Antimicrobial properties of composite films

The Table 4 reports the bactericidal results of samples composed by TPE-E AgNPs@ ZnO/SiO_2, (TPE-ENC) according to standard test JIS Z 2801.

The pristine TPE-E polymer showed no bactericidal activity as expected for either two types of tested bacteria. The sample obtained by extrusion TPE-ENC1 stands out, which showed a significant result with a bacterial reduction of 92% for *S. aureus* and 93% for *E. coli*. The samples that presented best bactericidal activity results were those produced by compression molding, TPE- ENC3, and TPE-ENC4 and TPE-ENC5. Between those, the sample irradiated at 50 kGy had the better efficacy.

The highest bactericidal efficiency (Reduction) for TPE-ENC5 was values of 98% for *S.aureus* and 96% for *E.coli*. The irradiation promotes improvements in the activity due to modification in the surface of the films and in consequence exposition of silver nanoparticles. The values of bactericidal activity between non-irradiated and irradiated with 20 kGy (TPE-ENC4) and 50 kGy (TPE-ENC5) showed a discrete change. According to the literature [46, 48] studies of colloidal silver nanoparticles obtaining via ^{60}Co gamma radiation in irradiated PVA, in N_2 atmosphere, of mean size of 29.7 nm with spherical geometry, presented significant results against *P.aeruginosa*, *E. coli*, *C. albicans* and *S. aureus*, in cotton fabrics. The dose of 35 kGy, at radiation rate of 5.65 kGy.h^{-1}, improved the efficiency.

Although it is not clear the main mechanism to explain the effects observed on the surfaces of the compression molded samples, two factors can operate in this effect: The surfaces of the compression molding samples are degraded by compression temperature allowing to Ag° diffusion. The slightly degradation caused by the radiation, confirmed by Tonset, in terms of chain scission, corroborates with the nanosilver diffusion, and other the direct

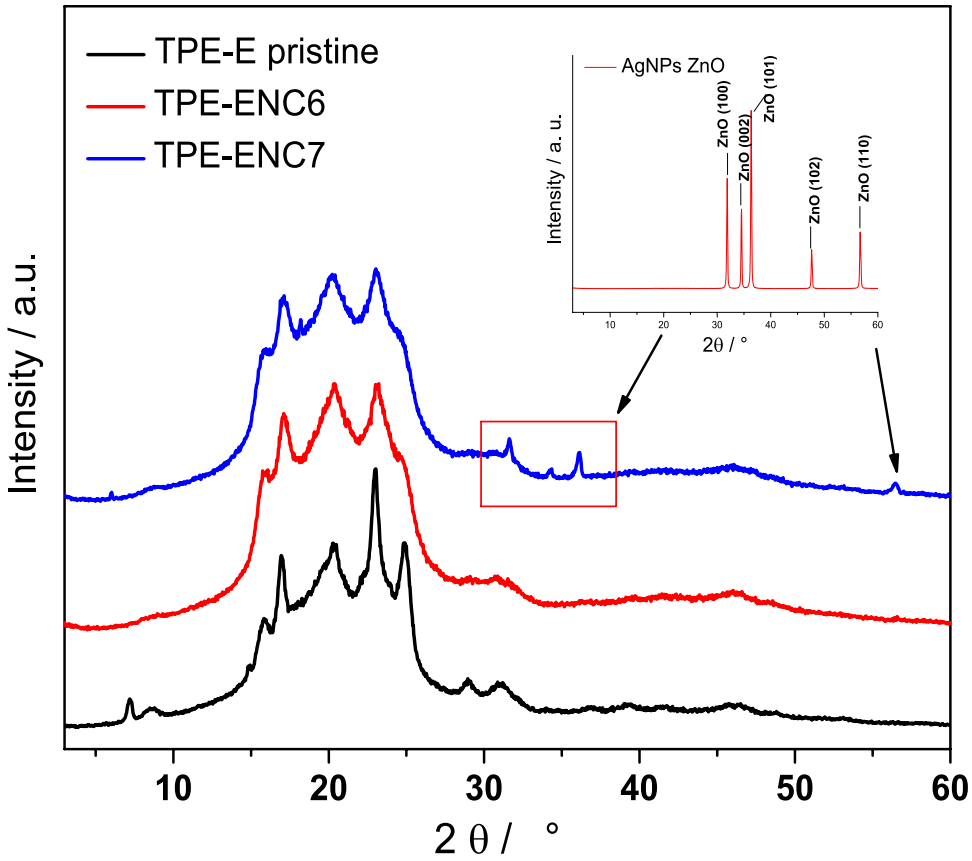

Fig. 10 XRD Diffractogram of samples from injection process: pristine TPE-E, TPE-ENC7 and TPE-ENC6. The inset show XRD pattern for the prepared Ag@ZnO nanoparticles

surface silver radiation can reduce it in nanoparticles improving the bactericidal effect.

4 Conclusions

Microscopic analysis suing SEM and TEM show the efficient anchoring of the AgNPs nanoparticles on SiO_2 and good distribution of the zinc and silver nanoparticles.

The films obtained by injection in the concentrations 0.05 and 0.5% of AgNPs@ZnO/SiO_2 (TPE-E6 and 7) showed the lowest result of biocidal activity in comparison with other processed samples. AgNPs@ZnO/SiO_2 films obtained by compression molding with and without irradiation (TPE-E3, 4 and 5) showed higher activity levels than the films processed in single screw extruder containing 0.05 and 0.5 AgNPs@ZnO/SiO_2 (TPE-E1 and 2). The compression method resulted in samples with the best indexes of bactericidal activities, followed by the single extrusion method and finally the injection method.

Considering the effects observed on the surfaces of the thermally compressed samples, two factors can operate: the surfaces of the compression molding samples are degraded by compression temperature allowing to Ag° diffusion, where the slightly degradation caused by the

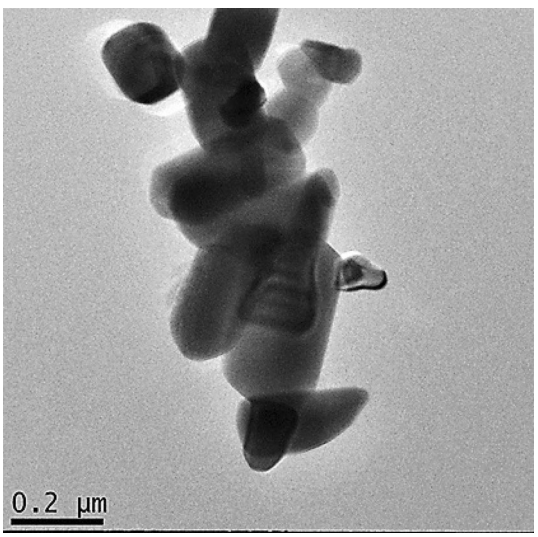

Fig. 11 TEM image of AgNPs@ZnO/SiO_2 powder nanoparticles

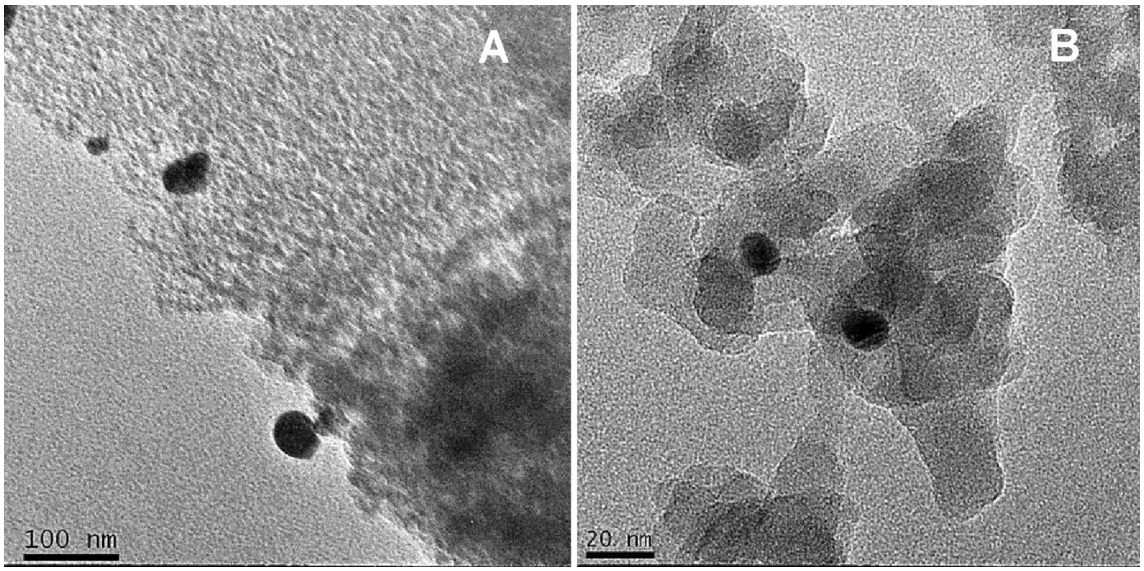

Fig. 12 TEM microphotographs of TPE-E AgNPs/SiO_2 nanoparticles

radiation corroborated also with Ag° diffusion as modified in Tonset temperature, and silver exposed to radiation can be reduced to nanoparticles for bactericidal activity.

The gamma irradiation causes the increased intensity of vibrational modes, the crystallite size and lattice strain were reduced and modified. This phenomenon creates defects in the polymer corroborating the better interaction by contact of nanoparticles with microorganisms.

The irradiation applied to the surface of pressed films favored the antimicrobial activity, also for exposing the nanoparticles more efficiently to the superficial level as effect of irregularities formation. The mechanism for release of metal ions (Ag^+) is the corrosion of nanoparticles present in the bulk of the TPE-E owing to the diffusion of water molecules. TPE-E is hydroscopic due to their polar character, allowing the diffusion of water molecules through holes of microscale defects induced by gamma radiation. Finally the efficiency of the bactericidal activity of TPE-E films depends on the incorporation process as well as the concentration of AgNPs on the polymer.

Table 4 Results of bactericide activity essay of TPE-ENC: Bacterial reduction rate, R (%) index

Sample	*S.aureus*		*E.coli*	
	Reduction/%	R	Reduction/%	R
TPE-E Pristine	0	0	0	0
TPE-ENC1	92	1.11	93	1.19
TPE-ENC2	76	0.62	75	0.60
TPE-ENC3	97	1.59	96	1.40
TPE-ENC4	93	1.18	94	1.26
TPE-ENC5	98	1.70	96	1.44
TPE-ENC6	55	0.35	56	0.36
TPE-ENC7	55	0.37	57	0.36

1:0.05/EXT; 2:0.5/EXT; 3:0.5/CM; 4:0.5/CM20; 5:0.5/CM50; 6:0.05/INJ; 7:0.5/INJ

Acknowledgements The authors acknowledge the financial support for this work from CAPES (process number 8881.068030/2014-10), CNPQ, CNEN-IPEN. The author Duclerc F Parra acknowledges the bilateral project's support between the IPEN and the University of Tuskegee, Alabama, USA. The author Washington L Oliani acknowledges the Materials Science and Technology Center—CCTM-IPEN for microscopy analysis (FESEM and TEM). The authors Leonardo G Marchini and Camila Basseti acknowledge to Pablo Vasquez for utilization of multipurpose gamma irradiation facility at the Radiation Technology Center—CTR-IPEN and Luiz G H Komatsu thanks to ControlBio by antimicrobial activity tests.

Compliance with ethical standards

Conflict of interest The authors declare that they have no conflict of interest.

References

1. Maynard LA, De-Butts BL, Barone JR (2019) Mechanical and thermal properties of polyolefin thermoplastic elastomer blend. Plast Rubber Compos 48(8):338–346
2. Wang W, Lu W, Goodwin A, Wang H, Yinb P, Kanga NG, Hong K, Mays JW (2019) Recent advances in thermoplastic elastomers from living polymerizations: macromolecular architectures and supramolecular chemistry. Progr Polym Sci 95:1–31
3. Fink JK (2011) Handbook of engineering and specialty thermoplastics, thermoplastic copolyester elastomers. Scrivener Publishing LLC, Wiley, New Jersey, pp 377–427
4. Bardin A, Gac PYL, Cérantola S, Simon G, Bindi H, Fayolle B (2020) Hydrolytic kinetic model predicting embrittlement in thermoplastic elastomers. Polym Degrad Stab 171:109002
5. Jiang R, Chen Y, Yao S, Liu T, Xu Z, Park CB, Zhao L (2019) Preparation and characterization of high melt strength thermoplastic polyester elastomer with different topological structure using a two-step functional group reaction. Polymer 179:121628
6. Amin S, Amin M (2011) Thermoplastic elastomeric (TPE) materials and their use in outdoor electrical insulation. Rev Adv Mater Sci 29:15–30
7. Manas D, Mizera A, Navratil M, Manas M, Ovsik M, Sehnalek S, Stoklasek P (2018) The electrical, mechanical and surface properties of thermoplastic polyester elastomer modified by electron beta radiation. Polymers 10:1057
8. Fijan S, Turk SŠ (2012) Hospital textiles are they a possible vehicle for healthcare-associated infections. Int J Environ Res Public Health 9:3330–3343
9. Pray L (2008) Antibiotic resistance, mutation rates and MRSA. Nat Edu 1:1–30
10. Haque M, Sartelli M, McKimm J, Bakar MA (2018) Health care-associated infections-an overview. Infec Drug Resist 11:2321–2333
11. Cabral FW, Silva MZO (2013) Infection prevention and control in the hospital environment. Sanare Sobral 12:59–70
12. Alvarez-Lonrenzo C, Bucio E, Burillo G, Concheiro A (2010) Medical devices modified at the surface by ray grafting for drug loading and delivery. Exp Opin Drug Deliv 7(2):7173–7185
13. Laporte RJ (2010) Hydrophilic polymer coating for medical devices – structure, properties, development, manufacture and application. CRC-Press, Taylor, New York, p 198
14. Asadinezhad A, Novak I, Lehocky M, Bilek F, Vesel A, Junkar I, Saha P, Popelka A (2010) Polysaccharides coatings on medical grade PVC: a probe into surface characteristics and the extent of bacterial adhesion. Molecules 15:1007–1027
15. Kumar R, Howdle S, Munstedt H (2005) Polyamide/silver antimicrobials: effect of filler types on the silver ion release. J Biom Mater Res Part B Appl Biomat 75:311–319
16. Oliani WL, Parra DF, Lima LFCP, Lugao AB (2015) Development of a nanocomposite polypropylene with biocide action from silver nanoparticles. J Appl Polym Sci 132(29):42218
17. Jo Y, Garcia CV, Ko S, Lee W, Kim JT (2018) Characterization and antibacterial properties of nanosilver-applied polyethylene and polypropylene composite films for food packaging applications. Food Biosci 23:83–90
18. Rao Y, Banerjee D, Datta A, Das SK, Guin R, Saha A (2010) Gamma irradiation route to synthesis of highly re-dispersible natural polymer capped silver nanoparticles. Rad Phys Chem 79(12):1240–1246
19. Triebel C, Vasylyev S, Damm C, Stara H, Ozpinar C, Hausmann S, Peukert W, Munstedt H (2011) Polyurethane/silver-nanocomposites with enhanced silver ion release using multifunctional invertible polyesters. J Mater Chem 21:4377–4383
20. Tomacheski D, Pittol M, Simoes DN, Ribeiro VF, Santana RMC (2017) Effect of natural ageing on surface of silver loaded TPE and its influence in antimicrobial efficacy. Appl Surf Sci 405:137–145
21. Tomacheski D, Pittol M, Ribeiro VF, Santana RMC (2016) Efficiency of silver- based antibacterial additives and its influence in thermoplastic elastomers. J Appl Polym Sci 133(37):43956
22. Pittol M, Tomacheski D, Simoes DN, Ribeiro VF, Santana RMC (2017) Antimicrobial performance of thermoplastic elastomers containing zinc pyrithione and silver nanoparticles. Mater Res 20:1266–1273
23. Mahamuni-Badiger PP, Patil PM, Badiger MV, Patel PR, Thorat-Gadgil BS, Pandit A, Bohara RA (2020) Biofilm formation to inhibition: role of zinc oxide-based nanoparticles. Mater Sci Eng C 108:110319
24. Khatoon N, Alam H, Khan A, Raza K, Sardar M (2019) Ampicillin silver nanoformulations against multidrug resistant bacteria. Sci Rep 9:6848
25. Hussain M, Ko YH, Choa YH (2016) Significant enhancement of mechanical and thermal properties of thermoplastic polyester elastomer by polymer blending and nanoinclusion. J Nanomater. https://doi.org/10.1155/2016/8515103
26. Yang W, Ma L, Song L, Hu Y (2013) Fabrication of thermoplastic polyester elastomer/layered zinc hydroxide nitrate nanocomposites with enhanced thermal, mechanical and combustion properties. Mat Chem Phys 141:582–588
27. Nagai Y, Ogawa T, Nishimoto Y, Ohishi F (1999) Analysis of weathering of a thermoplastic polyester elastomer II, factors affecting weathering of a polyether-polyester-elastomer. Polym Degrad Stab 65:217–224
28. Aleksandrovic V, Djonlagic J (2001) Synthesis and characterization of thermoplastic copolyester elastomers modified with fumaric moieties. J Serb Chem Soc 66:139–152
29. DIN EN ISO 527–1, (2019) Plastics — Determination of tensile properties – Part1: General Principles, Benth-Verlag, Berlin
30. Oburoglu N, Ercan N, Durmus A, Kasgoz A (2012) Effects of filler type on the nonisothermal crystallization kinetics of poly(butylene-terephthalate) (PBT) composites. J Appl Polym Sci 123:77–91
31. Righetti MC, Di-Lorenzo ML, Angiuli M, Tombari E, La-Pietra P (2007) Poly(butylene-terephthalate)/poly(ε-caprolactone) blends: Influence of PCL molecular mass on PBT melting and crystallization behavior. Eur Polym J 43:4726–4738
32. JIS Z 2801 (2010) Japanese Standard Association. Antibacterial Products – Test for Antibacterial Activity and Efficacy, 3rd english edn. Tokyo
33. Deshmukh GS, Peshwe DR, Pathak SU, Ekhe JD (2014) Nonisothermal crystallization kinetics and melting behavior of poly(butylene terephthalate) (PBT) composites based on different types of functional fillers. Thermochimica Acta 58:141–153
34. Kim K, Cha J, Yun SW, Gong MS (2015) Preparation of zinc oxide nanoparticles at low temperature using new organometallic zinc carbamate precursor. Bull Korean Chem Soc 36:1426–1432
35. Doan Q, Nguyen MH, Sai CD, Pham VT, Mai HH, Pham NH, Bach TC, Nguyen VT, Nguyen TT, Ho KH, Tran TH (2020) Enhanced optical properties of ZnO nanorods decorated with gold nanoparticles for self cleaning surface enhanced Raman applications. Appl Surf Sci 505:144593
36. Raju NRC, Kumar KJ (2011) Photodissociation effects on pulsed laser deposited silver oxide thin films: surface enhanced resonance Raman scattering. J Raman Spectrosc 42:1505–1509
37. Alfaro JAA, Valdes SS, Valle LFR, Ortiz HO, Nonell JM, Soto APP, Cespedes RIN, Mercado YAP, Belmontes FA (2013) Ultrasound irradiation coating of silver nanoparticles on ABS sheet surface. J Inorg Organomet Polym 23:673–683

38. Piedade AP, Pinho AC, Branco R, Morais PV (2020) Evaluation of antimicrobial activity of ZnO based nanocomposites for the coating of non- critical equipment in medical-care facilities. Appl Surf Sci 513:145818
39. Roberson M, Rangari V, Jeelani S (2014) Synthesis and characterization silver, zinc oxide and hybrid silver/zinc oxide nanoparticles for antimicrobial applications. Nano Life 4(1):1440003
40. Manas D, Mizera A, Manas M, Ovsik M, Hylova L, Sehnalek S, Stoklasek P (2018) Mechanical properties changes of irradiated thermoplastic elastomer. Polym (Basel) 10(1):87
41. Georgekutty R, Seery MK, Pillai SC (2008) A highly efficient Ag-ZnO photocatalyst: synthesis, properties, and mechanism. J Phys Chem 112:13563–13570
42. Rojas K, Canales D, Amigo N, Montoille L, Cament A, Rivas LM, Gil-Castell O, Reyes P, Ulloa MT, Ribes-Greus A, Zapata PA (2019) Effective antimicrobial materials based on low-density polyethylene (LDPE) with zinc oxide (ZnO) nanoparticles. Compos Part B 172:173–178
43. Oliani WL, Lima LFCP, Rogero SO, Riella HG, Lugao AB, Parra DF (2015) AgNPs polypropylene gel films thermal study and antibacterial activity. J Therm Anal Calorim 119:1963–1970
44. Martínez JR, Palomares-Sánchez S, Ortega-Zarzosa G, Ruiz F, Chumakov Y (2006) Rietveld refinement of amorphous SiO_2 prepared via sol–gel method. Mater Lett 60:3526–3529
45. Bakhori SKM, Mahmud S, Mohamad D, Masudi SM, Seeni A (2019) Surface morphological and mechanical properties of zinc oxide eugenol using different types of ZnO nanopowder. Mater Sci Eng C 100:645–654
46. Lee SH, Jun BH (2019) Silver nanoparticles: synthesis and application for nanomedicine. Int J Mol Sci 20(4):865
47. Agnihotri S, Mukherji S, Mukherji S (2014) Size-controlled silver nanoparticles synthesized over the range 5–100nm using the same protocol and their antibacterial efficacy. RSC Adv 4:3974–3983
48. Bera A, Garai P, Singh R, Gupta PP, Malav S, Singh D, Kumar D, Tiwari BL, Vaijapurkar SG (2015) Gamma radiation synthesis of colloidal AgNPs for its potential application in antimicrobial fabrics. Rad Phys Chem 115:62–67